

Toward ultra high magnetic field sensitivity $\text{YBa}_2\text{Cu}_3\text{O}_{7-\delta}$ nanowire based superconducting quantum interference devices

M. Arzeo, R. Arpaia, R. Baghdadi, F. Lombardi, and T. Bauch^{a)}

Quantum Device Physics Laboratory, Department of Microtechnology and Nanoscience (MC2), Chalmers University of Technology, SE-412 96 Göteborg, Sweden

(Received 8 January 2016; accepted 20 April 2016; published online 5 May 2016)

We report on measurements of $\text{YBa}_2\text{Cu}_3\text{O}_{7-\delta}$ nanowire based Superconducting QUantum Interference Devices (nanoSQUIDs) directly coupled to an in-plane pick-up loop. The pick-up loop, which is coupled predominantly via kinetic inductance to the SQUID loop, allows for a significant increase of the effective area of our devices. Its role is systematically investigated and the increase in the effective area is successfully compared with numerical simulations. Large effective areas, together with the ultra low white flux noise below $1 \mu\Phi_0/\sqrt{\text{Hz}}$, make our nanoSQUIDs very attractive as magnetic field sensors. *Published by AIP Publishing.*

[<http://dx.doi.org/10.1063/1.4948477>]

I. INTRODUCTION

Recent advances in nano-technologies applied to cuprate High critical Temperature Superconductors (HTS) have made it possible to realize nanowire based Superconducting QUantum Interference Devices (nanoSQUIDs) with extremely high magnetic flux sensitivity characterized by white flux noise values $S_\Phi^{1/2}$ below $1 \mu\Phi_0/\sqrt{\text{Hz}}$.^{1,2} Such devices might pave the way for the study of nano-magnetism at high magnetic fields with the ultimate goal of single spin detection.³ Here the high flux sensitivity is achieved by the small inductance of the SQUID loop.⁴ However, other prominent SQUID applications, such as magneto encephalography^{5,6} and low field magnetic resonance imaging,⁷ require a low magnetic field noise, $S_B^{1/2}$, which is given by $S_B^{1/2} = S_\Phi^{1/2}/A_{\text{eff}}$, with A_{eff} the effective area of the device. In this respect, bare nanoSQUIDs have a rather poor magnetic field sensitivity due to their small loop area. In order to keep the low flux noise, i.e., the small SQUID loop, one can increase the effective area of the device by directly coupling the nanoSQUID loop to a much larger pick-up loop. This approach has been already employed for grain boundary Josephson junctions (JJs) based HTS SQUID,^{8,9} and proven to allow for an at-will increase of the effective area without altering the inductance of the SQUID loop. Here it is important to note that such a feature is not possible with the implementation of a SQUID washer, where the SQUID inductance increases with the effective area.¹⁰ Moreover, the simplicity of the single layer deposition and single patterning process makes the pick-up loop approach more attractive compared with an inductively coupled multi-turn flux transformer. However, the noise mechanisms in nanowire based SQUIDs as well as the effect of a pick-up loop, coupled to this kind of nanoSQUID, on the overall noise performance have not been previously studied.

In this work, we present results from the measurement of $\text{YBa}_2\text{Cu}_3\text{O}_{7-\delta}$ (YBCO) nanoSQUIDs, realized in Dayem

bridges configuration,^{1,11,12} directly coupled to an in-plane magnetic field pick-up loop. The pick-up loop allows for a significant increase of the effective area (A_{eff}) of our devices, which is in a very good quantitative agreement with numerical calculations. Our calculations provide a more accurate estimation of the effective area, in comparison with the approximated expression commonly used in literature.^{9,10} The presence of the pick-up loop does not affect the magnetic flux noise performances of our nanoSQUIDs with values for the white flux noise below $1 \mu\Phi_0/\sqrt{\text{Hz}}$. These devices are, therefore, very appealing for future applications as magnetic field detectors.

II. DEVICE LAYOUT AND FABRICATION

Figure 1 shows the Scanning Electron Microscope (SEM) images of a typical nanoSQUID galvanically connected to an in-plane pick-up loop. For the realization of these devices, a 50 nm thick YBCO film (false colors) is deposited by Pulsed Laser Deposition (PLD) on a (110) MgO substrate (dark regions). Both the nanoSQUID (orange region) and the pick-up loop (green region) are then patterned via Ar^+ ion milling, through an e-beam lithography defined hard carbon mask. More details of the nanopatterning procedure are described in Refs. 13 and 14. For this experiment, the width and the length of the two nanowires have been fixed to 65 nm and 200 nm, respectively (see Fig. 1). The nanowires work as bridges between a 1 or 2 μm wide (d_w) electrode and the pick-up loop, whose inner diameter (d) ranges from 40 to 400 μm . The electrical transport properties of the devices are measured at low temperature in a ³He cryostat, properly shielded from ambient magnetic field. The single nanowires are characterized by high critical current densities J_C in the range $3\text{--}6 \times 10^7 \text{ A/cm}^2$ at $T = 5 \text{ K}$, which are typical values for YBCO nanostructures realized with our nanopatterning technique.^{14,15} Moreover, they operate up to a critical temperature $T_C \simeq 83 \text{ K}$, very close to the one of the as grown YBCO film ($T_C \simeq 85 \text{ K}$).

^{a)}E-mail: thilo.bauch@chalmers.se

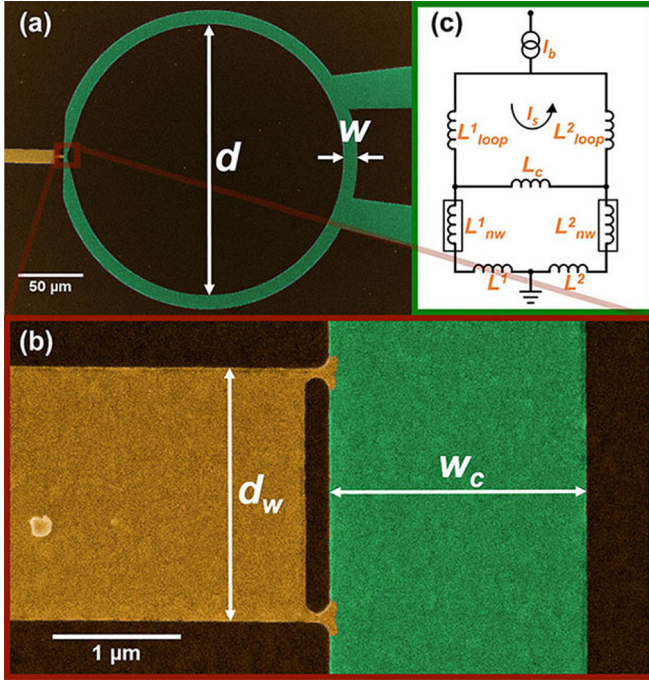


FIG. 1. Scanning electron microscope images of a typical device. Here, the YBCO is depicted in false colors (orange and green regions), whereas the dark regions represent the MgO substrate. (a) Overview of the entire device, highlighting the shape and the size (diameter d and width w) of the pick-up loop (green region). (b) Zoom-in, showing the details of the device in the vicinity of the nanowires: a narrow electrode (orange) and part of the pick-up loop (green), connected by the two nanowires, form the nanoSQUID loop. The distance between the two wires and the width of the pick-up loop in the vicinity of the nanowires are d_w and w_c , respectively. (c) Circuit schematic of the presented devices. The different parts are represented by inductive elements. In particular, the nanowires are represented by the inductances L^1_{nw} and L^2_{nw} . The pick-up loop inductance is given by the sum $L_{loop} = L_c + L^1_{loop} + L^2_{loop}$ and the nanoSQUID loop inductance by the sum $L^1_{nw} + L^2_{nw} + L_c + L^1 + L^2$. The bias and the screening current are denoted with I_b and I_s , respectively.

III. RESULTS AND DISCUSSION

A. Effective area analysis

We first discuss the influence of the pick-up loop on the effective area of the nanoSQUID. The effective area represents the portion of the device that contributes to magnetic flux when an external magnetic field B_a is applied. It can be experimentally determined from the measurement of the modulation period ΔB of the SQUID's voltage-field (or critical current-field) characteristic, as expressed by the formula: $A_{eff}^{exp} = \Phi_0 / \Delta B$, where $\Phi_0 = h/2e$ is the magnetic flux quantum. The experimental effective area does not correspond to the nanoSQUID hole geometric area, which in our specific case is given by the product of the separation between the nanowires and their length l (see Fig. 1(b)): $A_{geo} = d_w \cdot l$. This is due to the fact that the total phase difference between the two wires is enhanced by the contribution of the superconducting phase gradient $\nabla\phi$ induced by the screening current I_s circulating in the electrodes or, as in this case, in the pick-up loop when an external magnetic field is applied. This extra phase gradient is therefore responsible for an A_{eff}^{exp} larger than A_{geo} .

An analytic expression for the effective area, A_{eff}^{an} , can be obtained by means of an interacting loop-currents model for superconducting networks in the presence of magnetic field,¹⁶ satisfying the fluxoid quantization condition.¹⁷ Our devices can be represented by an equivalent circuit as sketched in Fig. 1(c), where the different parts act as inductive elements. By minimizing the total energy of the system and keeping the vorticity of the pick-up loop at zero (number of fluxoid quanta in the pick-up loop is zero), we get the following expression for the effective area:

$$A_{eff}^{an} = A_{nS} + A_{eff}^{pl} \frac{L_c}{L_{loop}}, \quad (1)$$

where A_{nS} is the effective area of the nanoSQUID in absence of the pick-up loop, A_{eff}^{pl} is one of the pick-up loops, and L_c and $L_{loop} = L_c + L^1_{loop} + L^2_{loop}$ are, respectively, the coupling and the total pick-up loop inductance (see Fig. 1(c)). The latter can be approximated using analytic expressions for a thin superconducting film¹⁸

$$L'_{loop} = \frac{\mu_0 \lambda_L}{w} \coth\left(\frac{t}{\lambda_L}\right) + \frac{\mu_0}{2\pi} \left[\ln\left(\frac{16r}{w}\right) - 2 \right]$$

$$L'_c = \frac{\mu_0 \lambda_L}{w_c} \coth\left(\frac{t}{\lambda_L}\right) + k/2, \quad (2)$$

where μ_0 is the vacuum permeability, λ_L is the London penetration depth, t is the thickness of the YBCO film, w and r are the average radius and width of the pick-up loop, respectively, and w_c is the width of the YBCO strip where the two loops meet (see Fig. 1(b)). Finally, $k \simeq 0.3$ pH/ μ m is an empirical expression for a slit inductance per unit length, obtained from measurements and simulations.¹⁹ The geometric term of L'_c is, hence, approximated as half slit inductance. Here the prime sign indicates that Equations (2) are per unit length. In both Equations (2), the first term is associated to the kinetic energy of the charge carriers (kinetic inductance L_i^{kin}) and the internal magnetic field energy, the second one (geometric inductance L_i^{ex}), instead, to the energy from the external magnetic field. Equation (1) infers that the coupling inductance L_c plays the major role, determining the amount of magnetic flux transferred from the pick-up to the nanoSQUID loop. For this reason, in order to enhance this effect on the A_{eff} of the devices, the pick-up loop, in the proximity of the nanowires, is 2 μ m wide, whereas it widens up to 10 μ m over a distance of $\simeq 30$ μ m from them (see Fig. 1). Here, it is important to point out that for our devices the kinetic contribution dominates over the geometric one.²⁰

The geometric term, in fact, accounts only for roughly 34% of the total coupling inductance at $T = 5$ K, becoming even less significant at higher temperatures. Indeed, at $T = 77$ K, it accounts only for roughly 7% of L_c , with a ratio $L_c^{kin}/L_c^{ex} \simeq 14$ (see Fig. 2). This behavior in temperature strongly indicates that the coupling between the nanoSQUID and the pick-up loop takes place mainly via kinetic inductance.

A more accurate estimation of the effective area of our devices can be obtained by numerically solving the London

and Maxwell equations²¹ in the presence of an externally applied magnetic field B_a . The current distributions inside the SQUID structure were calculated assuming the pick-up loop in the zero flux state (zero vorticity) and, without loss of generality, zero circulating current in the small SQUID loop. The effective area of the device can then be estimated from the computation of the fluxoid value around the nanoSQUID loop, Φ' , and the applied field: $A_{eff}^{num} = \Phi'/B_a$. The temperature dependence can be taken into account by using a modified two-fluid model for $\lambda_L(T) = \lambda_0/\sqrt{1 - (T/T_c)^n}$, with $n \simeq 2$.²²

In Figure 2, we plot the experimentally determined effective area A_{eff}^{exp} versus the inner diameter (d) of the pick-up loop, for devices with nanowires separation of $1 \mu\text{m}$ (orange circles) and $2 \mu\text{m}$ (green diamonds). In the same figure, the solid and the dashed lines represent A_{eff}^{num} and A_{eff}^{an} , respectively. As shown in the figure, the experimental data are in a much better agreement with the numerical calculations compared with values obtained analytically using Equations (1) and (2). This demonstrates that the numerical method can be used for a more accurate and useful computational pre-study of any future device modification, regarding both sizes and geometry, aiming at improved device performances. To perform the numerical simulations as described, prior knowledge of the device dimensions and of

the London penetration depth value for our YBCO films is required. The actual dimensions of each device have been extracted from SEM images as illustrated in Refs. 13 and 15, whereas we get the best fitting of the experimental data shown in Fig. 2 using a $\lambda_0 \simeq 150 \text{ nm}$ at $T=5 \text{ K}$ ($\lambda_L \simeq 400 \text{ nm}$, obtained from a modified two-fluid model with $T_c=83 \text{ K}$ and $n=2$, is used for fitting data at $T=77 \text{ K}$). Such values differ from typical λ_L extracted for YBCO nano-devices.^{23,24} This could be due to the much larger lateral dimensions of the pick-up loop and so of the entire device, resulting in a λ_L comparable with the one for bulk YBCO. On the contrary, any value of λ_L in the range $150\text{--}260 \text{ nm}$ does not allow for a good fitting of the experimental data by means of Equations (1) and (2). This reflects an inaccuracy in the analytic expression for the geometric inductances L_i^{ex} . The inaccuracy would be more pronounced for more complex geometries, for which the estimation of the geometric inductances becomes very difficult.

B. Noise properties

We now focus on the characterization of the magnetic flux noise of the devices. The noise measurements have been performed in an open loop configuration and using a cross correlation scheme,²⁵ which results in an amplifier input white noise level of $\simeq 1.5 \text{ nV}/\sqrt{\text{Hz}}$. The latter value also includes the thermal noise from the resistive lines connecting the devices at low temperature to the room temperature amplifiers. The nanoSQUIDs are biased by a DC current slightly above the critical current (I_c) and by an external magnetic flux, which maximizes the value of $\partial V/\partial \Phi$. The flux noise density $S_{\Phi}^{1/2}$ is evaluated from the measurement of the voltage noise density $S_V^{1/2}$ as follows: $S_{\Phi}^{1/2} = S_V^{1/2}/V_{\Phi}$, where V_{Φ} is the transfer function defined as: $V_{\Phi} = \max(\partial V/\partial \Phi)$. In Figure 3(b) we show a typical spectral density of magnetic flux noise measured on a nanoSQUID, at $T=5 \text{ K}$. In particular, the reported measurement is taken at a DC bias current $I_b = 1.76 \text{ mA}$ and a flux bias such that $V_{\Phi} = 2.4 \text{ mV}/\Phi_0$, as shown in Figure 3(a). The flux noise is, in fact, frequency dependent in the entire range, with a value of about $100 \mu\Phi_0/\sqrt{\text{Hz}}$ at $f=10 \text{ Hz}$. At frequencies above 100 kHz , the flux noise is limited by the electronics background noise. Therefore, we take $S_{\Phi}^{1/2} \simeq 1 \mu\Phi_0/\sqrt{\text{Hz}}$ as the upper limit for the white noise of the device. This value is very close to the one previously reported for equivalent YBCO nanoSQUIDs in the absence of the pick-up loop.¹ The f -dependent noise is not related to the flux bias point, thence, it has to be attributed to the critical current fluctuations in our devices. Critical current fluctuations, in ordinary tunnel-like Josephson junctions (JJs), are usually associated to bistable charge trapping states in the junction barrier.^{26,27} In our nanowires instead, the critical current noise might be caused by fluctuations of the electronic nematic order.^{28,29} However, the detailed understanding of the physical mechanisms responsible for such behavior in our nanowires is not known yet and would require further systematic studies, which goes well beyond the scope of the present work. Nevertheless, for a more detailed and quantitative analysis of the measured magnetic flux noise, we have fitted the spectra to

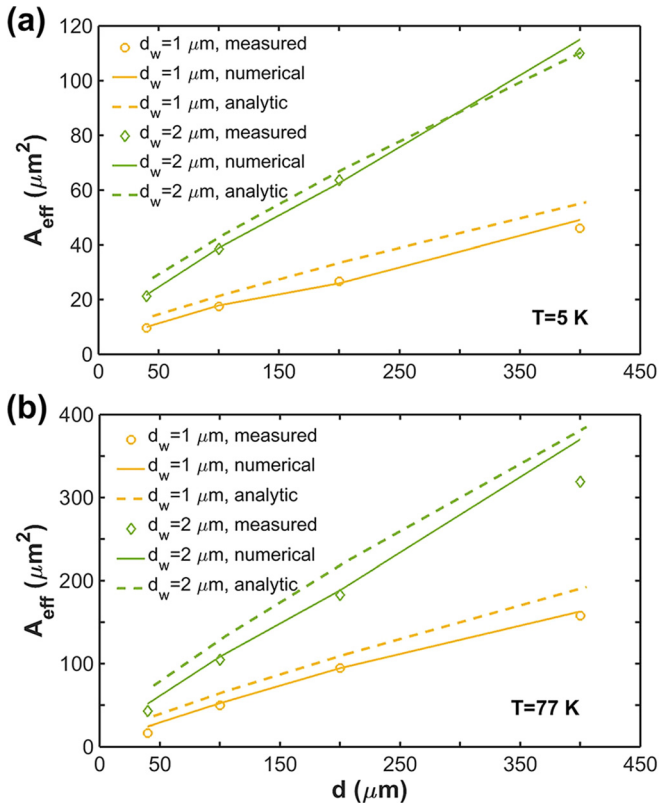


FIG. 2. Experimentally determined nanoSQUID effective area as a function of the pick-up loop diameter, for devices with a wires separation of $1 \mu\text{m}$ (orange circles) and $2 \mu\text{m}$ (green diamonds) at $T=5 \text{ K}$ (a) and at $T=77 \text{ K}$ (b). The solid and the dashed lines, representing, respectively, numerical and analytic calculations, obtained for the different reported device geometries, are presented for comparison. The extracted ratio between the kinetic and geometric coupling inductance values increases from 2 at $T=5 \text{ K}$ to 14 at $T=77 \text{ K}$.

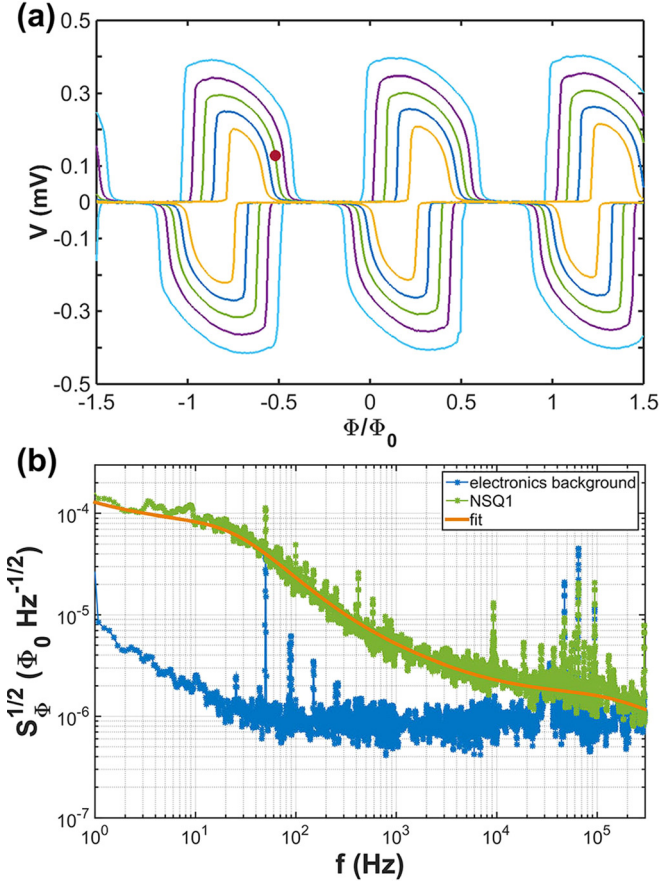


FIG. 3. (a) Voltage–flux characteristics at different DC bias currents and temperature $T = 5$ K. The dark red dot indicates the work point, at which the spectrum is taken ($I_b = 1.76$ mA), resulting in a transfer function $V_\Phi = 2.4$ mV/ Φ_0 . (b) Magnetic flux noise spectral density S_Φ as a function of the frequency f , measured in an open loop configuration, at $T = 5$ K, on a nanoSQUID with $d_w = 1$ μ m and coupled to a pick-up loop with an inner diameter equal to 100 μ m (NSQ1, green line). The red solid line represents the fit to $F(f)$ as described in the main text. The spectrum due to the electronics background noise is also plotted (blue line).

the sum of one or more Lorentzians $F_{L,i}^{1/2} = F_{0,i}^{1/2} / [1 + (f/f_{c,i})^2]^{1/2}$ with an amplitude $F_{0,i}^{1/2}$ and a characteristic frequency $f_{c,i}$, a contribution $F_{1/f}^{1/2} \propto 1/f^{1/2}$, and a constant white noise term $F_w^{1/2}$. As shown in Figure 3(b), our data are very well fitted by the expression $F^{1/2}(f) = \sqrt{\sum_i F_{L,i} + F_{1/f} + F_w}$. For the presented measurement, we have used two Lorentzians, for which we extract $f_{c,1} = 25$ Hz, $F_{0,1}^{1/2} = 80 \mu\Phi_0 / \sqrt{\text{Hz}}$ and $f_{c,2} = 200$ kHz, $F_{0,2}^{1/2} = 1.4 \mu\Phi_0 / \sqrt{\text{Hz}}$, respectively, and a white noise $F_w^{1/2} = 0.8 \mu\Phi_0 / \sqrt{\text{Hz}}$. To remove the

contribution to the flux noise from critical current fluctuations and extend the low noise region down to lower frequencies, one would need a Flux-Locked Loop (FLL) configuration in combination with a bias reversal scheme.^{2,30} To study the influence of the pick-up loop on the nanoSQUIDs noise performances, we have characterized devices with different effective areas. In Table I we report the measured values of the magnetic flux white noise level, or the relative upper limit set by the read-out electronics, for the investigated devices. A summary of the main parameters for each nanoSQUID, including the dimensions and the transport properties, are also listed in Table I. Our results indicate that the white noise level is independent of the value of the effective area of the device. This suggests that a further increase of A_{eff} , by means of a bigger pick-up loop, will not result in a deterioration of the noise performances. This would allow the realization of nanoSQUIDs able to reach a magnetic field sensitivity in the range of $\text{fT}/\sqrt{\text{Hz}}$, which represents the ultimate goal for various applications.^{5–7,31}

IV. CONCLUSIONS

We have fabricated YBCO nanoSQUIDs in Dayem bridges configuration implementing high quality nanowires. The electrical transport properties of these devices are characterized by a high reproducibility. The nanoSQUIDs are directly coupled to an in-plane pick-up loop, which allows for an at-will increase of the effective area of the devices. The amount of magnetic flux transferred from the pick-up to the nanoSQUID loop depends on the coupling inductance L_c . In particular, the coupling takes place mainly via kinetic inductance as inferred from the temperature dependence of the effective area. The influence of the pick-up loop, on both the effective area and the noise performances, has been systematically investigated. The experimentally determined effective area has been successfully compared with numerical calculations based on the Maxwell and London equations. The model can be further implemented to simulate the device behavior with modifications in the design and dimensions. The magnetic flux noise spectra for the investigated devices are frequency dependent up to hundreds of kHz (limit set by the read-out electronics bandwidth). This f -dependent noise is attributed to critical current fluctuations and can be described by the sum of Lorentzians, $1/f$ -like, and white noise spectra. However, an important point is that the white flux noise level of our nanoSQUIDs is independent of the dimensions of the pick-up loop and, thence, of the effective area. These results make our devices very attractive for applications requiring a magnetic field sensitivity in the $\text{fT}/\sqrt{\text{Hz}}$ range, and thus a very large effective area. This

TABLE I. Parameters of some investigated nanoSQUIDs, characterized by different effective areas. The actual dimensions are obtained from SEM images of the devices. V_Φ is the value of the transfer function at the work point used for the noise measurement at $T = 5$ K. I_c and $\delta R = \partial V / \partial I$ are, respectively, the critical current and the differential resistance, extracted from the IV characteristics, with a voltage criterion of $V = 2$ μ V; $S_{\Phi,w}^{1/2}$ is the magnetic flux white noise upper limit of the device, as set by the electronics background noise. NSQR is a device without pick-up loop reported for comparison.¹

Device	d_w (μ m)	l (nm)	w (nm)	d (μ m)	A_{eff} (μm^2)	I_c (mA)	δR (Ω)	V_Φ (mV/ Φ_0)	$S_{\Phi,w}^{1/2}$ ($\mu\Phi_0/\sqrt{\text{Hz}}$)	$S_{B,w}^{1/2}$ (pT/ $\sqrt{\text{Hz}}$)
NSQ1	1	200	65	100	24	1.7	0.8	2.4	<1	<86
NSQ2	1	200	65	400	62	2.4	2.4	0.75	<2	<66
NSQR	1	100	65	...	2.8	1.75	0.2	1.5	<1	<740

could be achieved by using larger coupling inductances and a larger pick-up loop. As an example, increasing the pick-up loop diameter by a factor of 20 (i.e., $d \simeq 8$ mm) and the coupling inductance L_c by a factor of 5 should result in a field noise of $100 \text{ fT}/\sqrt{\text{Hz}}$.

ACKNOWLEDGMENTS

This work has been partially supported by the Swedish Research Council (VR) and the Knut and Alice Wallenberg Foundation. We acknowledge support from the Marie Curie Initial Training Action (ITN) Q-NET 264034.

- ¹R. Arpaia, M. Arzeo, S. Nawaz, S. Charpentier, F. Lombardi, and T. Bauch, *Appl. Phys. Lett.* **104**, 072603 (2014).
- ²T. Schwarz, R. Wölbing, C. F. Reiche, B. Müller, M. J. Martínez-Pérez, T. Mühl, B. Büchner, R. Kleiner, and D. Koelle, *Phys. Rev. Appl.* **3**, 044011 (2015).
- ³C. Granata, A. Vettoliere, R. Russo, M. Fretto, N. De Leo, and V. Lacquaniti, *Appl. Phys. Lett.* **103**, 102602 (2013).
- ⁴J. Gallop, *Supercond. Sci. Technol.* **16**, 1575 (2003).
- ⁵M. Hämäläinen, R. Hari, R. J. Ilmoniemi, J. Knuutila, and O. V. Lounasmaa, *Rev. Mod. Phys.* **65**, 413 (1993).
- ⁶M. Xie, J. Schneiderman, M. Chukharkin, A. Kalabukhov, S. Whitmarsh, D. Lundqvist, and D. Winkler, *IEEE Trans. Appl. Supercond.* **25**, 1 (2015).
- ⁷V. M. Zotev, A. N. Matlashov, P. L. Volegov, I. M. Savukov, M. A. Espy, J. C. Mosher, J. J. Gomez, and R. H. Kraus, Jr., *J. Magn. Reson.* **194**, 115 (2008).
- ⁸M. Matsuda, Y. Murayama, S. Kiryu, N. Kasai, S. Kashiwaya, M. Koyanagi, T. Endo, and S. Kuriki, *IEEE Trans. Magn.* **27**, 3043 (1991).
- ⁹D. Koelle, A. H. Miklich, F. Ludwig, E. Dantsker, D. T. Nemeth, and J. Clarke, *Appl. Phys. Lett.* **63**, 2271 (1993).
- ¹⁰*SQUID Sensors: Fundamentals, Fabrication and Application*, Series E: Applied Sciences Vol. 329, edited by H. Weinstock (Kluwer Academic Publishers, 1996).
- ¹¹D. S. Hopkins, D. Pekker, P. M. Goldbart, and A. Bezryadin, *Science* **308**, 1762 (2005).
- ¹²C. Granata and A. Vettoliere, *Phys. Rep.* **614**, 1 (2016).
- ¹³R. Arpaia, S. Nawaz, F. Lombardi, and T. Bauch, *IEEE Trans. Appl. Supercond.* **23**, 1101505 (2013).
- ¹⁴S. Nawaz, R. Arpaia, F. Lombardi, and T. Bauch, *Phys. Rev. Lett.* **110**, 167004 (2013).
- ¹⁵S. Nawaz, R. Arpaia, T. Bauch, and F. Lombardi, *Physica C* **495**, 33 (2013).
- ¹⁶C. C. Chi, P. Santhanam, and P. E. Blöchl, *J. Low Temp. Phys.* **88**, 163 (1992).
- ¹⁷F. London, *Superfluids* (Wiley, 1950), Vol. 1.
- ¹⁸T. Van Duzer and C. Turner, *Principles of Superconductive Devices and Circuits* (Prentice Hall, 1999).
- ¹⁹M. Ketchen, *IEEE Trans. Magn.* **27**, 2916 (1991).
- ²⁰J. Johansson, K. Cedergren, T. Bauch, and F. Lombardi, *Phys. Rev. B* **79**, 214513 (2009).
- ²¹M. M. Khabaev, *Supercond. Sci. Technol.* **10**, 389 (1997).
- ²²W. Rauch, E. Gornik, G. Sölkner, A. A. Valenzuela, F. Fox, and H. Behner, *J. Appl. Phys.* **73**, 1866 (1993).
- ²³R. Arpaia, D. Golubev, R. Baghdadi, M. Arzeo, G. Kunakova, S. Charpentier, S. Nawaz, F. Lombardi, and T. Bauch, *Physica C* **506**, 165 (2014).
- ²⁴R. Arpaia, S. Charpentier, R. Toskovic, T. Bauch, and F. Lombardi, *Physica C* **506**, 184 (2014).
- ²⁵M. Sampietro, L. Fasoli, and G. Ferrari, *Rev. Sci. Instrum.* **70**, 2520 (1999).
- ²⁶C. T. Rogers and R. A. Buhrman, *Phys. Rev. Lett.* **53**, 1272 (1984).
- ²⁷D. Gustafsson, F. Lombardi, and T. Bauch, *Phys. Rev. B* **84**, 184526 (2011).
- ²⁸Y. L. Loh, E. W. Carlson, and K. A. Dahmen, *Phys. Rev. B* **81**, 224207 (2010).
- ²⁹E. W. Carlson and K. A. Dahmen, *Nat. Commun.* **2**, 379 (2011).
- ³⁰D. Drung, *Supercond. Sci. Technol.* **16**, 1320 (2003).
- ³¹A. Chwala, J. P. Smit, R. Stolz, V. Zakosarenko, M. Schmelz, L. Fritzsche, F. Bauer, M. Starkloff, and H.-G. Meyer, *Supercond. Sci. Technol.* **24**, 125006 (2011).